N87-27206

NONDESTRUCTIVE SEM FOR SURFACE AND SUBSURFACE WAFER IMAGING

Roy H. Propst, C. Robert Bagnell, Edward I. Cole Jr., Brian G. Davies,
Frank A. DiBianca, Darryl G. Johnson, William V. Oxford, and Craig A. Smith
University of North Carolina at Chapel Hill
Chapel Hill, NC

Abstract

The scanning electron microscope (SEM) is considered as a tool for both failure analysis as well as device chacterization. A survey is made of various operational SEM modes and their applicability to image processing methods on semiconductor devices.

I. Introduction

The SEM has become a standard tool for inspection and analysis in the semiconductor industry. Secondary (SE), voltage contrast (VC), electron beam induced current (EBIC), cathodoluminescence (CL) modes, as well as others, including time-resolved capacitive coupling voltage contrast (TRCCVC), provide both static and dynamic methods for investigation. Data from any of the methods are readily digitized into 512 X 512 pixel images. Although each image represents one quarter megabyte of data, image processing can be performed in or near real time.

We have developed processing methods which are particularly suited, but not unique, to semiconductor wafers and devices. The overall goal of our effort has been to show feasibility for various methods which can be used during fabrication as well as after-the-fact analysis.

The SEM is a versatile tool which can provide electrical parameters and topographic information during fabrication. Image processing can be used to enhance both visual and automatic pattern recognition.

II. Image Processing Storage and Retrieval

A. Introduction

Our research is focused on the application of different processing algorithms to Scanning Electron Microscope (SEM) images of integrated circuits. The primary goal is to develop a system to enable failure analysis of integrated circuits using the SEM as a non-destructive analysis tool. The result is the integration of diverse processing methods into a flexible, open-ended and easy-to-use data acquisition and processing system. We have investigated the use of both spatial and temporal domain processing techniques. The former techniques have proved

to be the most practical in terms of IC failure analysis purposes. We continue to evaluate new methods in both domains for data acquisition and processing.

Our present hardware comprises two separate systems. The first is a DEC PDP-11/23 minicomputer, coupled with an AED 512 graphics terminal and various A/D and D/A peripherals. This system controls the SEM and the Device Under Test (DUT) and is used for data acquisition and raw data storage. Another PDP-11/23 computer acts as a slave processor to the main 11/23 and is used to control the DUT when complex inputs are required. A block diagram of this system is shown in Figure 1. The second system is a DEC PDP-11/73, coupled with an AED 512 terminal, a video digitizer, and an array processor. This system is used for post-acquisition image processing and software development. The same software package operates on both systems, allowing total functionality with only one system if necessary.

B. Progress

Our work in this area can be divided into three main topics: 1) image acquisition and storage, 2) general processing routines and image data analysis, and 3) information display. The approach taken and the progress made in each of these areas will be discussed separately.

1) Image acquisition and storage

We have established a set of standard techniques for acquiring and storing data from the DUT. The major motivation was a quick and efficient transfer of only the required data from the DUT to the analysis computer. We have developed a method (node scanning) to accomplish this goal. Our findings were outlined in a paper which was published in the December 1985 issue of IEEE Transactions on Reliability.[1]

The basic concept behind node scanning is that a large portion of the area in present-day IC's is occupied by interconnections. Thus, only a small fraction of the area of a die needs to be sampled to determine the voltage present at each of the devices in the circuit. Only this voltage information is necessary in order to determine the operation of the circuit. Further, the raw image data from each of these "areas" (or nodes) can be analyzed and represented in a compact statistical format. Thus, the amount of information required to characterize the entire circuit can be reduced to a standard form which is independent of the actual device geometry. Since the ratio of "active" chip area to "passive" chip area varies widely with circuit design, so does the amount of data reduction using this technique. In this manner, data reduction factors of between 80 and 1300 over standard techniques can be realized. Figure 2 presents this relative data reduction as a function of device density. The major benefit of the node scanning technique is the increased throughput provided by the smaller amount of data which must be processed and analyzed. An additional benefit is the decreased amount of exposure of the DUT to the high-voltage primary electron beam, reducing the probability of damage to the device.

2) General Processing Routines and Image Data Analysis

The largest part of the system consists of a set of general image processing routines. These routines usually operate directly on the image data stored in the AED graphics terminal or on the combination of

AED data and additional data stored in disk files. Our investigation has concentrated on variations of common processing routines which work well with secondary electron (SE) and EBIC image data of IC's. Some of the capabilities we have implemented include image data filtering, addition, subtraction, multiplication, division, contrast enhancement, histogramming, and edge extraction.

One of our main objectives in applying the various processing algorithms to SEM image data is to separate the Voltage Contrast (VC) information from the topographic data. Since the SE signal is dependent on a large number of factors besides local electric fields, the extraction of "pure" voltage information from the SE signal is necessarily complicated. We have developed various image data subtraction techniques optimized for isolation of VC information from secondary images.[2]

Other difficulties associated with making repeatable measurements of voltage levels on the DUT are the non-deterministic characteristics (noise and drift) associated with the image data acquisition system. These factors have been examined in great detail[3] and techniques to minimize their effects have been proposed. In particular, image noise becomes an increasingly large component of the SE signal as the primary beam current is reduced to improve the temporal resolution of the capacitively coupled bound charge decay in a TRCCVC image (see next section). These elements must be dealt with using image processing techniques such as stroboscopic time averaging and filtering. Another aspect of system "drift" can be seen as geometric distortions of the image itself. We have implemented image translation, rotation, and scaling routines which we use to attempt to minimize these distortions. We have investigated various data interpolation methods to minimize the image distortions introduced by the rotation and scaling processes themselves. Edge-detection routines are useful in the detection of geometric shifts and the location of surface features. The performance of several different edge-detection methods on typical SE images has been examined. Image data analysis techniques such as histogramming and thresholded subtraction allow the extraction of data relevant to both the image processing phase as well as the operational analysis phase.

Another area of current interest is in frequency-domain techniques (such as Fourier transform filtering). An investigation of two-dimensional FFT processing for failure analysis and process quality monitoring is currently in progress. Presently, the use of FFT techniques for our image data processing is not desirable because of the computational and memory overhead involved in the FFT process. The majority of the image processing techniques which we use are based on simple 2 x 2 and 3 x 3 convolutions, which are more efficient to perform directly on the image data. We have implemented low-pass and high-pass FFT filtering and the results are nearly indistinguishable from direct convolution filtering. In the future, it may become desirable to perform some processing on the FFT rather than directly on the image data. For example, extremely narrow band-pass filtering is much more computationally efficient when performed using the FFT filtering approach. Thus, we will continue to investigate the applications of FFT image processing techniques.

We are also studying the application of Fourier Transform techniques to wafer and process quality evaluation. The monitoring of process quality directly from the two-dimensional FFT is a complex subject. Unfortunately, comparing the FFT's of two images is not directly

analogous to the more conventional approach of comparing two images, since it is not immediately clear how differences in process quality will affect the image, much less the FFT coefficients. In order to understand the relationship between wafer characteristics and the image FFT, the effects of different image acquisition conditions on the FFT have been investigated. The two-dimensional frequency coefficients are dramatically affected by different types of image data and imaging conditions. However, the underlying basic characteristics of the FFT of two images showing the same geometry remain unchanged even though the image contrast and signal-to-noise ratio may change dramatically. The main distinguishing feature of the FFT (the predominant line width) remains unchanged despite differences in the image acquisition conditions.

3) Image Information Display

The utility of using pseudo-color lookup tables for the display of gray-scale image data has been demonstrated many times. We have developed a facility to produce and modify our own color lookup tables interactively. This has enabled us to develop a set of color tables which is optimized for our purposes. The majority of our data is displayed using a modified Heated Object Spectrum (HOS) lookup table which runs from dark brown at the low end through red and yellow to white at the top end. This allows the use of color to enhance contrast perception but retains the intuitive "order" which is present in most gray-scale tables. In addition, we reserve a small set (typically 32) of pixel values at the top end of the table to allow image features to be marked or outlined and for alphanumeric labeling. These colors are generally "orthogonal" to the colors used in the HOS portion of the color table to allow easy differentiation.

A subroutine has been developed to map the three-dimensional image data function (X,Y and intensity) into a two-dimensional perspective view. This subroutine also includes primitive thresholding and data filtration features. The image intensity variable is represented as the vertical (Z) axis, and the normal X and Y coordinates are mapped into a perspective plane which is at 11 degrees to the CRT plane in the X direction and at 23 degrees inclination in the Y direction. These angles were chosen to enhance the visibility of image contrast features without losing a sense of the overall spatial proportions. Several options are available, allowing the user a choice of "front" or "rear" perspectives, data averaging, scaling, and windowing parameters, for enhancement of the resulting plot.

III. Time Resolved Capacitive Coupling Voltage Contrast

A. Introduction

Problems encountered using voltage contrast on passivated devices with a scanning electron microscope (SEM) have been well documented.[4-7] To avoid radiation damage from the primary electrons or the x-rays generated from these energetic electrons, low primary electron beam energies must be used. These electrons penetrate only into the uppermost

portion of the passivation layer.[8] A change in potential on a subsurface structure will polarize the insulating material between the structure and the surface. The bound surface charge associated with this polarization produces a transient in the secondary electron signal from the device. This signal can be used to generate a dynamic image-capacitive coupling voltage contrast. We have developed a new technique, Time Resolved Capacitive Coupling Voltage Contrast (TRCCVC), for determining the amplitude of this voltage transient. This technique relates the decay time of the dynamic voltage contrast flash to voltage transitions on a device. The decay times are also dependent on structure depth. Our techniques and initial results for depth measurement are also reported.

B. Signal Generation

A primary electron beam with energy > 100 eV will yield a secondary electron (SE) energy distribution whose shape is determined by the work function, Fermi level, and other material parameters.[9] There will be a net charge accumulation on the device if the primary beam current (I_{pe}) does not equal the loss current (I'). At the beam energies used for TRCCVC there are two major sources of I': SE and backscattered electrons (BE). The ratio of BE current to I_{pe}, η, is independent of incident beam energies greater than about 5 kV. At lower energies small variations with energy occur. The ratio (δ) of SE current to I_{pe} is dependent upon the material and the energy of the primary beam.[9] If the BE and SE currents exceed I_{pe}, as is the case for TRCCVC, a net positive charge will build up on the surface. This charge prevents lower energy SE's from escaping the surface and will thus decrease the intensity of the SE image. An equilibrium surface voltage is reached when there is no net charge accumulated on the device. When structures deeper than the maximum beam penetration depth change potential, the material between them and the surface is polarized, introducing a bound surface charge. The change in the number of SE's caused by this bound charge is the TRCCVC signal, which decays back to the equilibrium potential by permitting more or fewer SE to escape.

C. Data Acquisition and Voltage Results

Operating the SEM at standard TV video scan rates allowed the voltage contrast data to be videotaped and analyzed on a separate image processing system. The voltages applied to the DUT were square waves with variable period and amplitude. All periods were long enough to allow complete decay of the voltage contrast flash in the secondary electron image.

After the voltage contrast information had been recorded, decay data were obtained using a video-rate digitizer (Datacube Inc.). The digitizer converts the analog composite video signal into a digital array of 512 x 512 picture elements (pixels); each element has a signal resolution of eight bits. The resulting system has a maximum sampling rate of 33.3 msec (video rate of 30 frames per second).

Since the incident electron flux of the SEM primary beam is inversely proportional to the decay time of a given voltage contrast flash, the

primary electron beam current must be carefully chosen. The transient decay times must be long relative to the system sampling rate. The required flux level for adequate time resolution produced a poor signal-to-noise ratio in the secondary electron image (at the primary beam energy available on our SEM). To increase the signal-to-noise ratio, multiple frames of the voltage contrast flash, synchronous in time with the applied square wave, were averaged. The voltage contrast amplitude in the averaged secondary electron image was then determined as a function of time.

For sufficiently large voltage transients, a "saturation" effect of the dynamic voltage contrast signal occurs. The amplitude of the voltage contrast flash (and therefore the number of secondary electrons leaving the device surface) is constant for a time interval after the transition and before the onset of decay. The saturation parameters depend upon the SEM operating conditions as well as the work function and electron energy distribution of the passivation. Higher voltage shifts saturate at the same intensity but remain saturated for a longer time interval.

The monotonic relationship between saturation time and the amplitude of the negative voltage shift was used to make a voltage calibration curve. Using multiple frame averaging, the decay data for different voltage level transients were plotted. Following Menzel's suggestion[8] that the voltage contrast flash should decay exponentially, a least-mean-squares fit of the decay data (intensity-versus-time) to an exponential curve was calculated. The result was a series of exponential curves, each representing the decay of a given voltage level. The decay time required by any given flash to reach a fixed target intensity was then used to quantify the amplitude of the voltage pulse.

The samples used for voltage measurement were an npn power transistor and a Schottky diode with approximately 0.6 and 1.5 micrometers of passivation respectively. Initially voltage shifts from 1 to 5 V were recorded in 1 V steps. The decay time to the target intensity was then measured and the results plotted. By taking 1 V steps, the data acquisition time and SEM drift were both reduced. For higher voltage resolution, separate measurements were made over smaller ranges: 0.75-2.75V, 0.75-2.0V, 2.0-3.0V, 3.0-4.0V, and 4.0-5.0V (Figures 3 and 4). The SEM magnification was increased at higher voltage ranges to increase primary electron flux, and thereby decrease decay times. Table I shows experimental conditions and results. For transitions over the total 1-5 V range the maximum standard error is 106 mV. However, over 1 volt intervals the error varies from 16 to a maximum of 45 mV. These resolutions equal or surpass those published by Fujioka[10] using a SEM at 1.0 kV primary electron beam energy with an electron energy spectrometer accessory.

Table I. Experimental Conditions and Voltage Resolutions Using the Time Resolved Capacitive Coupling Voltage Contrast Technique on Two Different Devices.

Device	Primary Beam Energy (kV)	Sample Area ($pixels^2$)	Frames Averaged	Voltage Range (V)	Standard Error (mV)
Diode	2.50	64 x 64	14	1-5	58.5
Diode	2.50	64 x 64	10	0.75-2.75	28.5
Transistor	1.25	32 x 64	5	1-5	106.1
Transistor	1.25	32 x 64	5	0.75-2.00	44.8
Transistor	1.25	32 x 64	5	2-3	44.3
Transistor	1.25	32 x 64	5	3-4	34.6
Transistor	1.25	32 x 64	5	4-5	16.3

D. Modeling of Decay Data

In order to predict the shape of the SE decay curves, we must know the SE energy distribution, surface equilibrium voltage, and incident electron flux. Gorlich[11] suggests using closed form equations for the SE energy distribution, Eq. 1,[12] and for δ, Eq. 2[9]. In addition to these two equations, the time dependent potential on the surface, V(t), was predicted to decay like that across a capacitor in an RC circuit, i.e. Eq. 3.[11] The net absorbed current, I_{ae}, will be a function of the number of secondary electrons with energies greater than that of the surface potential (which is shown below in Eq. 4). It is obvious that even with Eq. 1 and 4, V(t) cannot be solved in closed form. An iterative solution can be formulated assuming V(t=0) is known (Eq. 5). Using constants for SiO_2[11,12] and typical SEM and device parameters in the above equations we have constructed the V(t) curves shown in Figure 5.

$$N = \frac{E_{se}}{(E_{se} + A)\,(E_{se} + F)^{y}} \qquad \text{Eq. 1.}$$

where: N = number of SE
E_{se} = energy of the SE
A, F, and Y are constants of the material
(A = Fermi level and F = work function)

$$\delta = (Q)^{-0.38}1.11\ \delta_{max}(1-\exp^{-2.3(Q)^{1.35}}) \qquad \text{Eq. 2.}$$

$$Q = E_{pe}/E_{pe\ max}$$

where: E_{pe} = primary beam energy
δ_{max} refers to δ value

$$V(t) = (d/A\mathcal{E}) \int_0^t I_{ae}\, dt \qquad \text{Eq. 3.}$$

where: $V(t)$ = surface voltage
$\mathcal{E}$ = permittivity of the material
A = area scanned
$I_{ae} = I_{se} + I_{be} - I_{pe}$
$d \triangleq$ structure depth

$$I_{ae} = \left[\delta \frac{\int_0^E N\, dE}{\int_0^{50} N\, dE} + \eta - 1.0 \right] I_{pe} \qquad \text{Eq. 4.}$$

$$V(t+\Delta t) = V(t) + \Delta t\, (d/A\mathcal{E})\, I_{ae}(V(t)) \qquad \text{Eq. 5.}$$

Qualitatively, the curves exhibit the same decay recorded earlier (including the "saturation" region). However, there are some problems with incorporating this approach into a quantitative model. First, the SE energy distribution of Eq. 1 does not consider the effects of surface contaminants. Second, the value of V(t=0), for a given voltage change on a device, will be a function of device depth, insulating material, and incident beam energy as well as the amplitude of the voltage change.

To improve on the exponential decay fit to our data, we have measured the integral SE distribution from the peak CCVC intensity after a voltage transition (Figure 6A). This intensity information is offset 3.4 volts such that the peak occurs at 0 volts. These data are then used in Eq. 4 above. The offset indicates an equlibrium surface voltage of 3.4 volts. Therefore, a -1 volt change on the surface would result in CCVC decay from 2.4 to 3.4 volts. The calculated decay curves and normalized data for V(t=0)=0.4, -0.6, -1.6 volts (-3, -4, and -5 volts device voltage changes respectively) are shown in Figure 6B. The -0.6 and -1.6 volt curves agree reasonably well with the measured data, but the 0.4 volt curve decay slower than the data. This discrepancy is probably a result of beam current drift, which is significant on our present SEM at low primary beam energies and beam currents (measured values for these data were 1.25 kV and .011 nA). These experiments and contamination effects will be examined on a new SEM, scheduled to arrive in June '86, more suited to our low accelerating voltage and low current research. Then the effects of drift and model deficiency can be separated.

E. Depth Measurement

Eq. 3 predicts that CCVC decay times should be inversely proportional to device depth (d). The TRCCVC decay data for two different areas on

the same die, each with -5 V transitions, were fitted to an exponential curve in the same manner as earlier data sets.[13] Two VC decay times over the same intensity range were then calculated from the exponential fit of each area. The passivation thickness over these areas was measured using a Nanometrics film gauge correlated to a Gaertner ellipsometer. The decay times and depths are 292 and 86 msec, and .549 and 1.580 micrometers, respectively. The ratios are:

$$\Delta t_1/\Delta t_2 = 3.40 \qquad \text{and} \qquad d_2/d_1 = 2.85.$$

From these ratios we see that while the relative depths and decay times agree with the inverse relation, the predicted and measured ratios differ by 16%. Part of this difference may be a result of the two areas being disimilar structures, oxide over metal and oxide over Si.

To eliminate this source of error, TRCCVC data for three different samples of the same die were examined. As can be seen in Figure 7, the decay data for these samples varied widely. Later measurements using the ellipsometer showed only a 2% difference in passivation thickness. We attribute the difference in signal to surface contaminants on each device, altering the SE energy distribution and the equilibrium voltage. Future experiments to eliminate surface contamination by plasma cleaning will be performed to see if these fluctuations in "identical" devices are eliminated. The fluctations must be resolved before quantitative depth and voltage measurements on different devices can be modeled.

F. Conclusions

We are developing a new technique, TRCCVC, for quantitative voltage and depth measurement of buried structures. The low primary beam energies used in this technique make it non-destructive, even to radiation sensitive MOS structures. Initial voltage calibration and qualitative decay modeling have been sucessful. However, the effects of surface contamination and SEM drift must be evaluated and/or eliminated before the overall goal, quantitative prediction of CCVC decay from SEM/device conditions, is achieved.

IV. Non-destructive Subsurface Imaging of Semiconductors

A. Introduction

The maximum penetration depth (R) of the primary beam-sample interaction volume in an SEM has been modeled as a function of the primary beam energy (E) and the atomic number and mass density of the sample.[14] In a silicon sample the dependence of R on the beam accelerating voltage may be approximated using the experimental range $R(E) = 0.022\ E^{1.65}$, where R is the maximum penetration depth in micrometers and E is the beam accelerating voltage in kV. The size, shape, and energy distribution of the beam-sample interaction volume are also affected by the beam accelerating voltage. We are investigating the effects of changes in beam energy on images obtained using different SEM imaging modes in order to evaluate the suitability of the SEM for non-destructive subsurface imaging of semiconductor devices.

SEM images of semiconductors may be obtained in one of two ways. The products of the elastic and inelastic scattering events occurring within the interaction volume may be measured using an external detector and used to modulate a display, resulting in an image related to the amplitude of a beam-induced emission from the sample. Alternatively, changes in the state of the sample itself induced by the primary beam-sample interactions may be measured and used to produce an image.

In order to compare SEM imaging modes, it is useful to represent each mode by a simplified "image function" model, I(x,y,E), where I represents the intensity of the image at a point (x,y) and E is the primary beam energy. We may think of I as the product of two component functions: I_g, which describes the number of events generated as a function of beam and sample parameters, and I_c, which describes the detection/measurement efficiency as a function of beam energy and penetration.

For example, the transfer of energy from primary beam electrons to weakly bound electrons in the sample results in the creation of low energy (< 50 eV) free electrons that may escape from the sample surface (secondary electrons or SE). The SE emission is measured and used to modulate the intensity of an x-y CRT display, resulting in a "secondary" image. For such an image, I represents the number of SE detected at a given location (x,y) with primary beam voltage E. I_g is proportional to the SE generation efficiency in the material(s) present in the sample and to the size and energy distribution of the interaction volume. The total SE generation efficiency is the sum of the weight fractions of each element present in the interaction volume weighted by the elemental SE generation efficiencies. The beam-sample interaction volume is roughly spherical or pear-shaped; free electrons are generated at all penetration depths r, $0 < r <= R$. The energy distribution within the interaction volume has been modeled as a spherical Gaussian distribution centered in the upper half of the sphere. I_e, which represents the probability that the SE escape the sample and are detected, is proportional to $\exp(-r/l_e)$, where l_e is the mean free electron path in the sample. Typical values for l_e are 1 nm for metals and 10 nm for insulators. This model, although approximate, is adequate to allow us to conclude that the SE mode is not well suited for subsurface imaging because of the low yield and rapid attenuation of the subsurface SE emission.

We have developed models similar to the above for imaging modes commonly available on standard SEMs: static voltage contrast, back-scattered electron imaging, TRCCVC (see previous section), cathodoluminescence, EBIC, and x-ray spectrometry. We have isolated TRCCVC, EBIC, and x-ray as the most promising for subsurface imaging, and are currently focusing our efforts on these methods.

B. Experimental Progress to Date

We have investigated the suitability of two SEM imaging modes, EBIC and windowed characteristic x-ray spectrometry, for the detection of subsurface structures. EBIC was used to detect buried P-N junctions in bipolar semiconductor devices. X-ray spectrometry was used to detect silicon layers buried underneath surface metallization.

For EBIC, as for SE, I_g is proportional to the free electron generation efficiency and the size and energy distribution of the interaction volume. Ie is proportional to $\exp(-d/l_m)$, where d is the

distance to the P-N junction at which the signal may be detected and l_m is the minority carrier diffusion length, which is typically much larger than l_e. Note that electrons do not have to escape the surface in order for a signal to be generated; we may measure EBIC current at P-N junctions buried in the bulk of the device.

The following is an example of experiments performed using EBIC to detect subsurface P-N junctions. The base and collector of a bipolar PNP transistor on a Honeywell 2171 test device were used as inputs to an EBIC detector/amplifier. Images of the EBIC signal were acquired as the primary beam voltage was ramped between 5 and 15 kV. At low beam voltages, an octagonal outline corresponding to the sides of the base-collector junction was visible. As the beam voltage was increased, an EBIC signal was detected from the interior of the octagonal region (Figure 8). This additional signal results from electron-hole pair production at the buried base-collector junction.[15]

We have applied this method to other devices with similar results. Beam penetration through silicon layers as well as surface passivation and metal layers has been observed. We were unable to detect structures at depths greater than approximately 6 micrometers because beam accelerating voltages greater than 30 kV are not available on the SEM used for these experiments. We expect that this method is applicable at greater penetration depths than were attainable using this instrument. We are currently investigating the qualitative potential of this method.

We have performed preliminary experiments using windowed characteristic x-ray spectrometry imaging to demonstrate beam penetration through surface metallization runs. For x-ray spectrometry, I_g is proportional to the elemental concentration within the interaction volume and to the primary beam overvoltage, $E - E_c$, over the energy range examined (E_c is the characteristic x-ray energy). I_e is a decreasing exponential function of distance and the elemental mass absorption coefficients. The use of energy windows to isolate characteristic x-rays greatly increases the sensitivity and resolution of the detection system.

The test device for these experiments was an NPN transistor on a depassivated Honeywell test device. A Kevex energy dispersive x-ray spectrometer interfaced to a multichannel integrator was used to measure the x-ray emissions. Energy windows 110 eV wide centered at 1.49 and 1.74 kV were used to detect the Al and Si K series characteristic x-rays. The SEM beam was scanned in a 256 x 256 raster pattern over the device; x-rays in each window were counted for 20 msec at each point of the image. The x-ray counts were used to modulate the intensity of a digital CRT display. Images were acquired with the SEM primary beam at voltages of 5, 10, 20, and 30 kV. At 5 and 10 kV, the silicon window image showed dark regions where the silicon layer was covered by the surface aluminum. As the beam voltage increased past 10 kV, the signal strength in these regions increased. We believe that this increase is caused by penetration of the primary beam through the metallization into the buried silicon layer.

C. Conclusions

We have evaluated the suitability of several common SEM imaging modes for non-destructive subsurface imaging of semiconductor devices. We are pursuing experimental investigation of three promising methods: TRCCVC, EBIC, and characteristic x-ray spectrometry, in an effort to

develop useful tools for efficient, non-destructive semiconductor quality control and fault analysis.

V. References:

[1]W.V. Oxford and R.H. Propst, IEEE Trans. on Reliability, Vol. R-34, No. 5, 410 (1985).

[2]R.H. Propst, C. Bagnell, E. Cole, B. Davies, and W. Oxford, SRC Quarterly Report, March 1984.

[3]F.A. DiBianca, C. Bagnell, E. Cole, D. Johnson, and W. Oxford, Scanning Electron Microscopy, Inc. I, 57 (1986).

[4]O.C. Wells, Appl. Phys. Lett. 14, 5 (1969).

[5]D.M. Taylor, J. Phys. D 11, 2443 (1978).

[6]L. Kotorman, Scanning Electron Microscopy, Inc. IV, 77 (1980).

[7]K. Ura, H. Fujioka, and K. Nakamae, Scanning Electron Microscopy, Inc. III, 1061 (1982).

[8]K.E. Menzel and E. Kubalek, Scanning 5, 103 (1983).

[9]H. Seiler, J. Appl Phys. 54(11), R1 (1983).

[10]H. Fujioka, K. Nakamae, and K. Ura, Scanning Electron Microscopy, Inc. III, 1157 (1983).

[11]S. Gorlich, K.D. Herrmann, and E. Kubalek, Proceeedings of the Microcircuit Engineering 84 Conference, Academic Press, 451 (1985).

[12]M.P. Seah, Surface Science 17, 132 (1969).

[13]E.I. Cole Jr., Appl. Phys. Lett. 48(9), 599 (1986).

[14]J.I. Goldstein et al., Scanning Electron Microscopy and X-Ray Microanalysis, Plenum Press, 53 (1981).

[15]Reimer, Scanning Electron Microscopy, Springer-Verlag, 286 (1985).

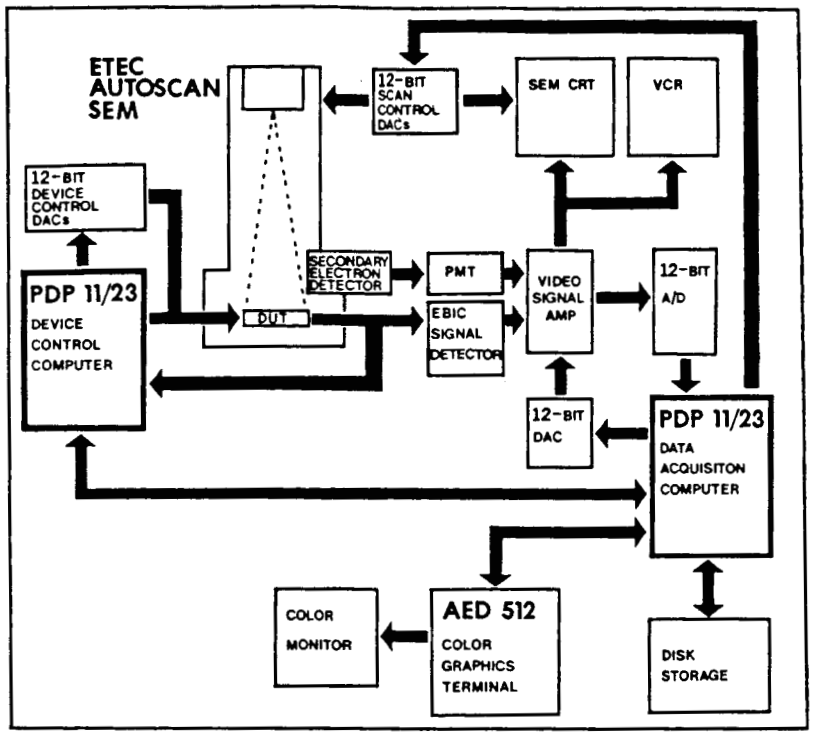

Figure 1. Block diagram of computer-controlled Scanning Electron Microscopy image acquisition system.

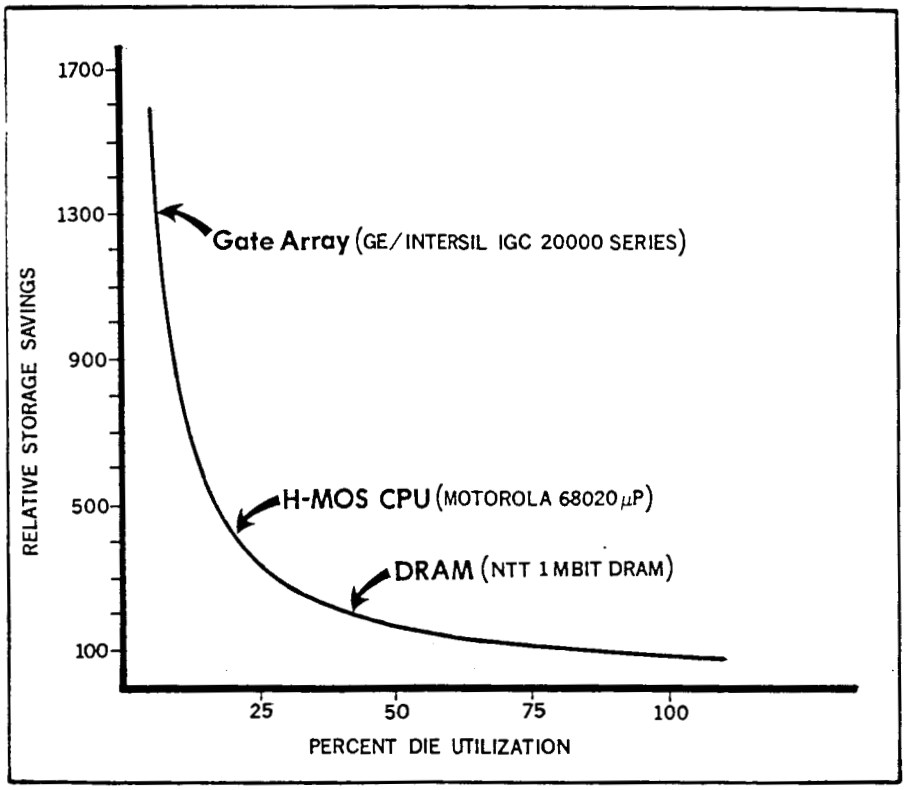

Figure 2. Data storage comparison between the node scanning method versus the whole image scanning method at different device densities.

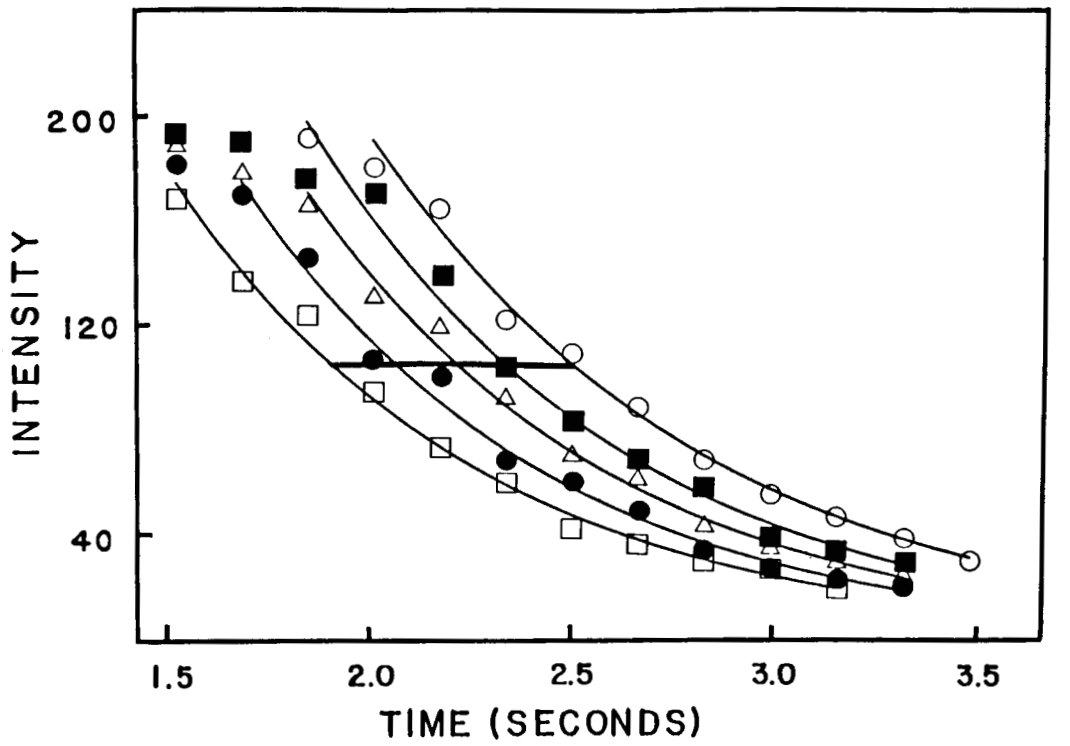

Figure 3. Measured decay data and best fit exponential curves for -4.0 to -5.0 volts applied transients. The line across the plot is the target intensity value.

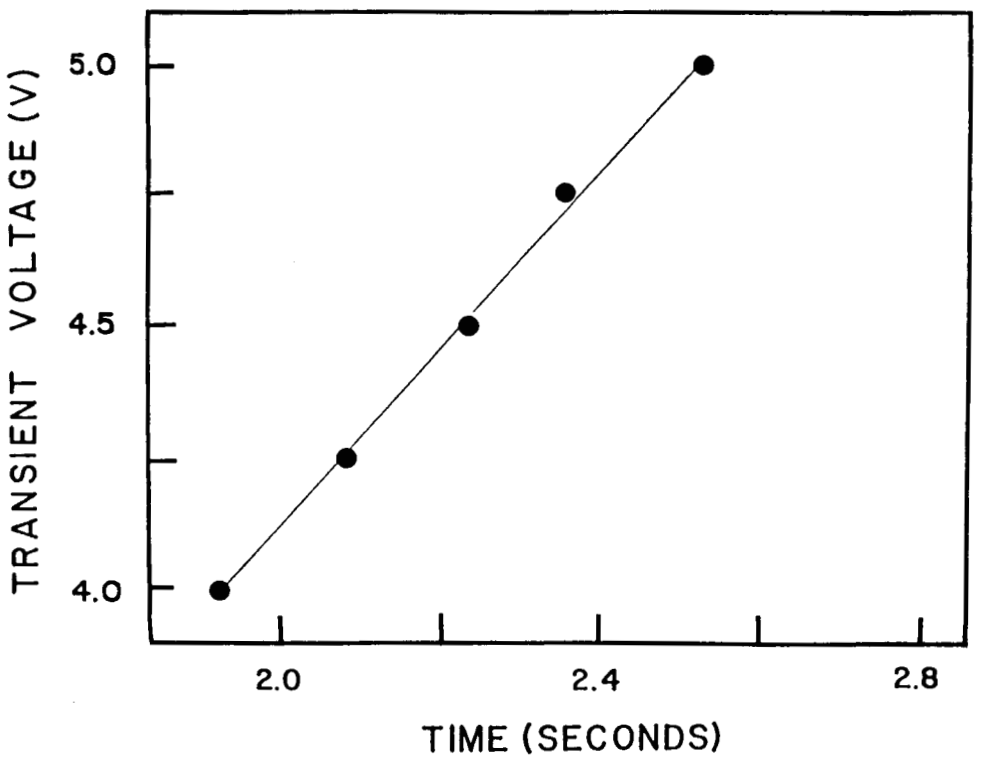

Figure 4. Time for an applied transient voltage to decay to the target intensity.

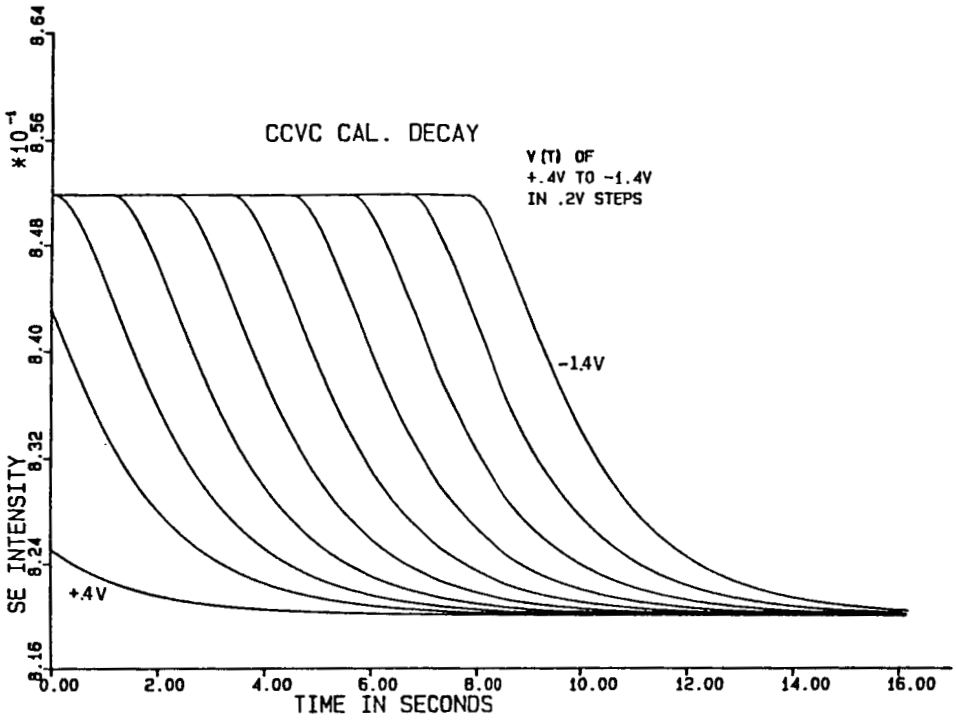

Figure 5. CCVC calculated decay curves from 0.4 to -1.4 volts initial surface voltage, 0.2 volt steps, using modeled SE energy distributions.

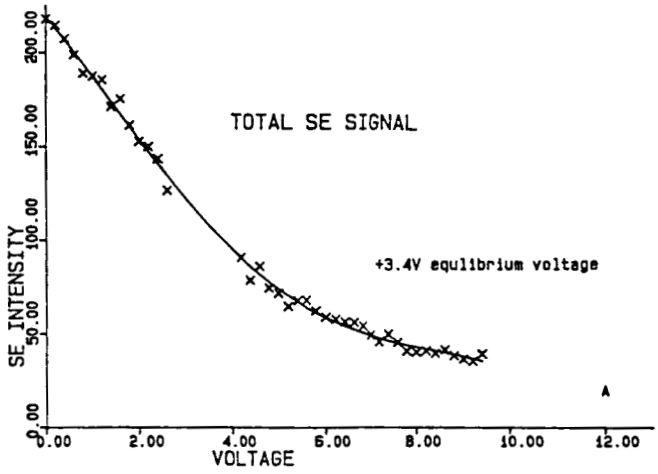

Figure 6A. Measured integral SE response with surface voltage.

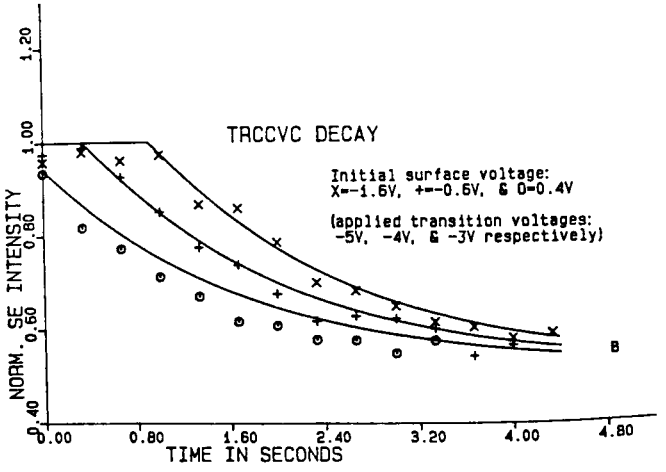

Figure 6B. Calculated CCVC decay curves from experimental integral SE energy distribution and decay data for 0.4, -0.6, and -1.6 volt initial surface voltages.

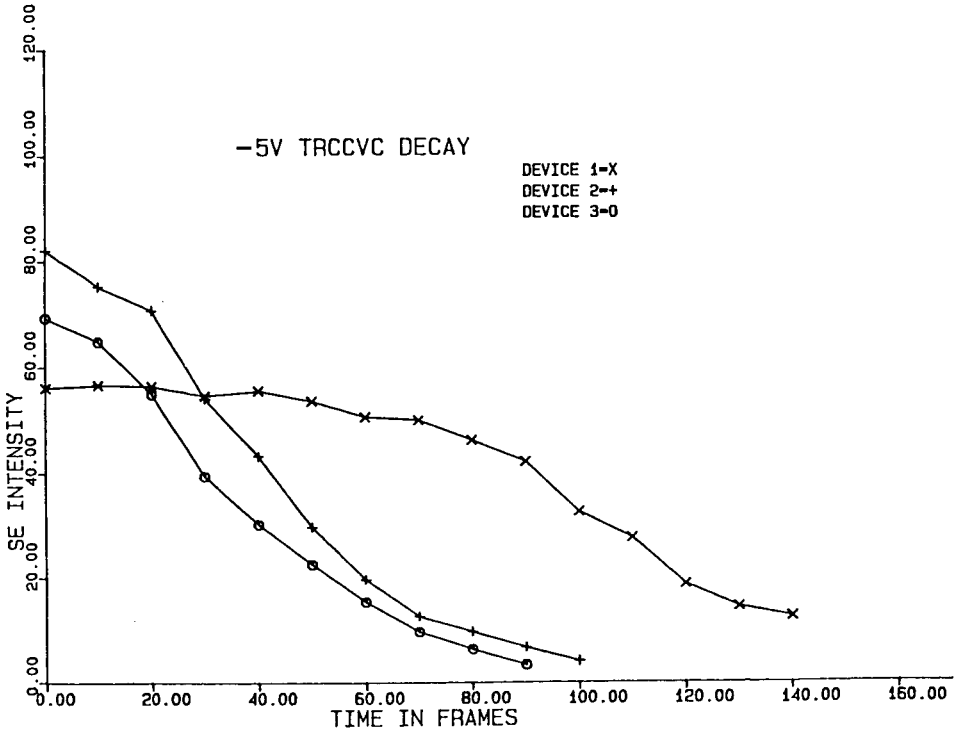

Figure 7. CCVC decay data for -5 volt applied transitions of the same device on different dies.

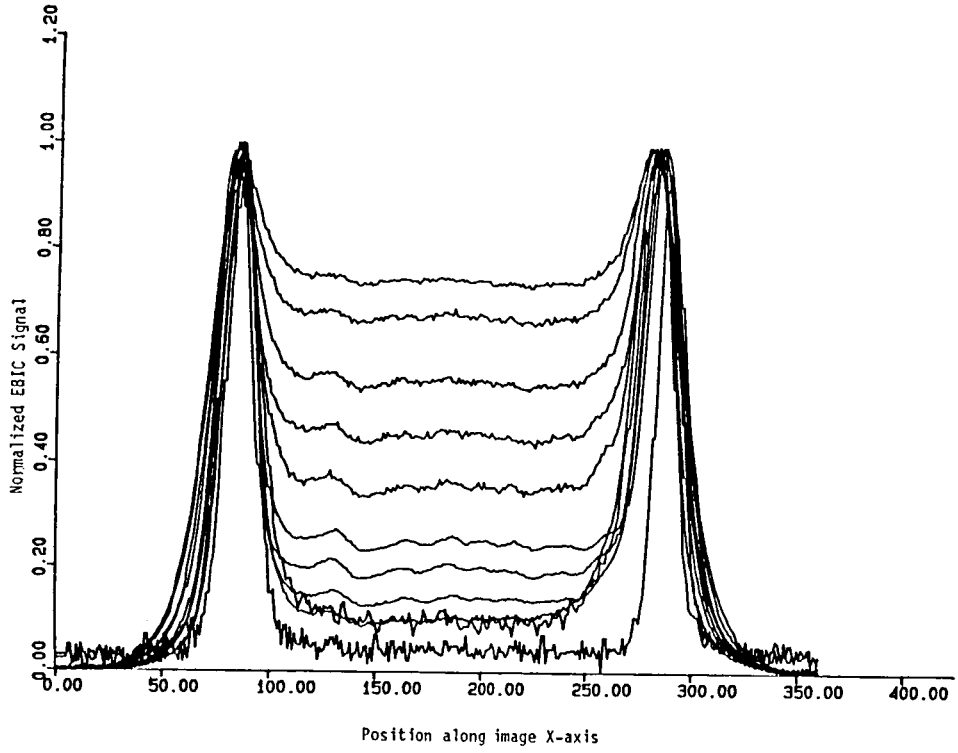

Figure 8. EBIC signal of base-collector junction at primary beam energies from 5-15 kV in 1 kV increments.